remote sensing

MDPI

Article

Surface Displacements Monitoring in Cyprus via InSAR and Field Investigation: The Case Studies of Pyrgos-Parekklisia and Pedoulas Villages

Stavroula Alatza [1,*], Constantinos Loupasakis [2], Alexis Apostolakis [1], Marios Tzouvaras [3,4], Kyriacos Themistocleous [3,4], Charalampos Kontoes [1], Chris Danezis [3,4] and Diofantos G. Hadjimitsis [3,4]

[1] National Observatory of Athens, Operational Unit BEYOND Centre for Earth Observation Research and Satellite Remote Sensing IAASARS/NOA, GR-152 36 Athens, Greece; alex.apostolakis@noa.gr (A.A.); kontoes@noa.gr (C.K.)
[2] Laboratory of Engineering Geology and Hydrogeology, School of Mining and Metallurgical Engineering, National Technical University of Athens, GR-157 80 Athens, Greece; cloupasakis@metal.ntua.gr
[3] ERATOSTHENES Centre of Excellence, Limassol 3012, Cyprus; marios.tzouvaras@cut.ac.cy (M.T.); k.themistocleous@eratosthenes.org.cy (K.T.); chris.danezis@cut.ac.cy (C.D.); d.hadjimitsis@cut.ac.cy (D.G.H.)
[4] Department of Civil Engineering and Geomatics, Cyprus University of Technology, Limassol 3036, Cyprus
* Correspondence: alatza@noa.gr

Abstract: The island of Cyprus is characterised by a complex geological environment as it overlies a boundary zone of three tectonic plates, leading to high seismicity and intensive tectonism. It consists highly of Neogene marls, exhibiting serious geotechnical problems due to their high content of clay minerals. Along with strong, destructive earthquakes, various geohazards have been identified in Cyprus, including landslides, swelling/shrinking phenomena and land subsidence etc. Pedoulas is a village in Cyprus experiencing ground deformation due to landslide phenomena. Conversely, Pyrgos and Parekklisia villages in Limassol, Cyprus are experiencing a long-term swelling/shrinking phenomenon. To further investigate this surface deformation, a time-series InSAR analysis of Sentinel-1 SLC images of ascending satellite passes was performed, with a parallelised version of PSI (Persistent Scatterers Interferometry), along with field investigation, for the time period of 2016 to 2021. Negative vertical displacements with maximum rates of −10 mm/y, were identified in Pedoulas village, while positive vertical displacements with a maximum rate of 10 mm/y, dominated in Pyrgos and Parekklisia villages. The analysis of precipitation data from 2017 to 2021, presented a correlation between annual fluctuations in precipitation in the affected areas and changes in the InSAR time-series deformation trends. In Pedoulas village, landslide movements sped up during spring and summer, when the infiltration of waste water in the ground intensified due to the increase in the tourist population. In Pyrgos-Parekklisia villages, higher positive deformation rates were identified in winter months, while during summer, when the formations dried out, uplifting phenomena stopped evolving. The integration of InSAR displacements with field investigation provided validation of the observed ground failures and added valuable insights into the driving mechanisms of the deformation phenomena. Finally, the assessment of the impact of the triggering factor in the evolution of the deformation phenomena, can serve as a valuable tool for risk mitigation.

Keywords: geohazards; earth observation; SAR interferometry; surface deformation; swelling/shrinking phenomena; Pedoulas; Pyrgos; Parekklisia

check for updates

Citation: Alatza, S.; Loupasakis, C.; Apostolakis, A.; Tzouvaras, M.; Themistocleous, K.; Kontoes, C.; Danezis, C.; Hadjimitsis, D.G. Surface Displacements Monitoring in Cyprus via InSAR and Field Investigation: The Case Studies of Pyrgos-Parekklisia and Pedoulas Villages. *Remote Sens.* **2024**, *16*, 960. https://doi.org/10.3390/rs16060960

Academic Editors: Timo Balz and José Fernández

Received: 8 December 2023
Revised: 16 February 2024
Accepted: 5 March 2024
Published: 9 March 2024

Copyright: © 2024 by the authors. Licensee MDPI, Basel, Switzerland. This article is an open access article distributed under the terms and conditions of the Creative Commons Attribution (CC BY) license (https://creativecommons.org/licenses/by/4.0/).

1. Introduction

Cyprus suffers intensively from the occurrence of numerous active landslides. As reported in the European landslide susceptibility map ELSUS V2, released through the European Soil Data Centre, up to 375 sites have been reported to be affected by slope movements since 2018 [1]. The majority of the slope damage involves the clayey or the

marly Neogene formations, mainly at the Paphos and Limassol regional districts [2], located at the southwest of the island.

Several geohazards, mainly rockfalls or slides along the weathering mantle, occur at the rock formations of the Troodos Mountain [3]. Nevertheless, during field investigation, ground deformations affecting building and linear infrastructure have also been identified in flat areas of very low to zero steepness, occupied by Neogene or Quaternary formations. As those areas cannot be affected by landslides, alternative driving mechanisms such as swelling/shrinking phenomena or subsidence due to the overexploitation of the aquifers should be investigated for their proper mitigation.

SAR interferometry, based on the ability to detect deformation on the Earth's surface through successive observations of the same area on the ground with different spatial and temporal baselines, is widely applied in a variety of geophysical applications. InSAR data were analysed to estimate co-seismic deformation [4–6]. The combination of InSAR and GPS data is also exploited to model seismic sources [7]. Wang et al. [8] employed InSAR co-seismic and multi-temporal InSAR post-seismic deformation to assess the seismic deformation mechanism. InSAR time-series techniques were also implemented [9,10] to achieve a more accurate earthquake modelling. Finally, owing to the global coverage and the large archive of Sentinel-1 data, Li et al. [11] developed an earthquake monitoring service using SAR interferometry. Volcano monitoring [12–14], glaciology [15], subsidence due to mining activities [16,17] and landslide monitoring [18] were also included in differential InSAR studies. Advances in SAR interferometry and the launch of new SAR satellites, enabled the use of multiple SAR acquisitions for monitoring long-term, slow-moving deformation phenomena. Specifically, the constellation of the Copernicus Sentine-1 A and B satellites, with the short revisit time and the wide spatial coverage, set a new era in remote sensing applications. Many techniques have been developed for InSAR time-series analysis. These techniques aim to identify coherent stable scatterers over long time periods. Based on the type of the identified scatterers, these techniques are divided in two main categories. The Permanent Scatterers Interferometry [19–21] and the Small Baselines Subset technique [22,23].

Multi-temporal InSAR techniques can provide valuable insights into historical and ongoing deformation phenomena, serving as a tool for identifying, monitoring and mapping a plethora of geohazards globally. InSAR techniques are widely applied in landslide monitoring [24–26]. Landslides can be detected using SBAS [27] and PSI techniques [28,29]. Furthermore, volcanic monitoring [30,31], tectonic activity [32–34], mining activities [35], monitoring deformation in dams [36], ground water level changes [37–41] and natural compaction [42,43] are some types of deformation geohazards where multi-temporal SAR interferometry is widely applied. During the last decade, the plethora of SAR data, especially the short revisit time of Sentinel-1 constellation combined with the wide spatial coverage, has enabled the monitoring of slow-moving, long-term deformation phenomena. InSAR time-series analysis provides diachronic insights on a wide variety of surface deformation phenomena, some of them previously unknown. In Cyprus, radar interferometry is used to monitor various types of ground instabilities or displacements, in combination with complementary satellite-based techniques and ground-based data [44–46]. However, many surface deformation phenomena in Cyprus are unidentified or require further investigation. Pedoulas and Pyrgos-Parekklisia villages in Cyprus are three areas that experience long-term surface displacement phenomena. Specifically, landslides are detected in Pedoulas village and swelling/shrinking phenomena exist in Pyrgos-Parekklisia villages.

To further investigate surface deformation in the above-mentioned villages, line of sight (LOS) surface displacements were estimated using Sentinel-1 images from 2016 to 2021. Furthermore, vertical displacements were estimated from the LOS deformation field. Field visits in the affected areas were performed to verify the observed ground damage. Failures in constructions were recorded on buildings in all three areas. Specifically, deforming permanent scatterers that derived from the InSAR time-series analysis were located on top of the building failures. To further investigate the triggering mechanism

of the deformation phenomena, an analysis of precipitations data was performed. A correlation between high annual precipitation rates and surface deformation was identified by analysing ERA-5 [47] land precipitation data covering the same time period as the LOS displacements. To assess the level of impact of extreme precipitation events on the initiation and evolution of deformation phenomena in Pedoulas, Pyrgos and Parekklisia villages, additional analysis of InSAR ground displacements and precipitation time-series analysis was performed. The assessment of the time lag between extreme precipitation events and the initiation of surface displacements, provided a deformation pattern and provided valuable insights into the driving mechanisms of the identified deformation phenomena.

In the present study, for the first-time, ground deformation phenomena in Pedoulas and Pyrgos-Parekklisia villages in Cyprus were mapped and monitored with the use of SAR interferometry techniques. Moreover, the investigation of the driving mechanisms of the identified LOS displacements provided added value in understanding the triggering factors of the observed surface deformation. Based on the InSAR measurements and the ERA-5 land weather data, a detailed analysis of the correlation between extreme precipitation rates and changes in the ground deformation patterns in the examined regions, was performed. An innovative aspect was the estimation of the time lag between the initiation of the deformation phenomena and fluctuations in precipitation rates. The knowledge of the impact of the triggering factor on the initiation of a geohazard, is of importance to risk mitigation. Therefore, early detection of geohazards and their triggering factors in Cyprus, by employing multi-disciplinary approaches can play a key role in risk assessment and risk reduction and serve as a valuable tool in monitoring geohazards in Cyprus.

2. Study Area: Geomorphology and Geological Setting

The present study aimed to investigate surface deformation in Cyprus by exploiting both satellite and ground truth observations to add valuable insights regarding the kinematic behaviour of the deforming areas of Pedoulas and Pyrgos-Parekklisia (Figure 1). Pedoulas, a popular summer resort, is located at an altitude of 1100 m on the northern flanks of the Troodos Mountain and at the highest planes of the Marathasa valley. It was founded on the weathering mantle of the gabbro rock of the Troodos ophiolite sequence, (mainly unlayered gabbro rocks, characterised by the lack of evidence for solid-state deformation [48,49]). The weathering mantle extends down to a depth of 10 to 15 m. This zone is susceptible to successive shallow rotational slides, with retrogressive characteristics. The villages of Pyrgos and Parekklisia are located at an altitude of 75 and 120 m, respectively, approximately 15 km east of Limassol. Both villages were founded on weathered pillow lavas alternating to the zeolitic phase (bentonitic clays with silt and radiolarite intercalations) and are susceptible to swelling/shrinking phenomena.

Figure 1. Pedoulas and Pyrgos-Parekklisia deforming sites in Cyprus.

3. Materials and Methods

3.1. Materials

To investigate surface deformation phenomena in Cyprus, three data sources were employed. Initially, SAR data from the Sentinel-1 sensor were analysed with the Stanford method of Persistent Scatterers Interferometry [20]. The generation of the interferometric stack was performed with ISCE v2 software [50,51]. LOS displacements were estimated for a 6 year time period from 2016 to 2021. The results of the PSI analysis were validated via ground truth investigations. Field visits were performed in the study areas in Cyprus to identify ground instabilities. Damage to many buildings in all three villages was detected. However, in the present study, only field observations that coincided with deforming scatterers, derived from the PSI analysis, were included. Finally, ERA-5 land precipitation data were analysed to investigate the correlation between extreme precipitation events and the observed surface deformation phenomena.

SAR Data

For InSAR time-series analysis in Cyprus, Sentinel-1 images covering the study areas of Pedoulas, Pyrgos and Parekklisia villages were selected. Sentinel-1 SLC images of ascending satellite pass no.160 (Figure 2) were processed with the Persistent Scatterers Interferometry technique to estimate LOS surface displacements. The short revisit time of the Sentinel-1 sensor enabled the exploitation of a quite dense archive of satellite data for InSAR time-series analysis in Cyprus. A set of 136 Sentinel-1 SLC images from an ascending satellite pass covering Cyprus from 2016 to 2021 were selected and processed. The primary

image from 10 June 2019 was selected based on the minimization of temporal and spatial baselines. Table 1 summarises all information about the Sentinel-1 data employed for InSAR time-series analysis in the study areas in Cyprus.

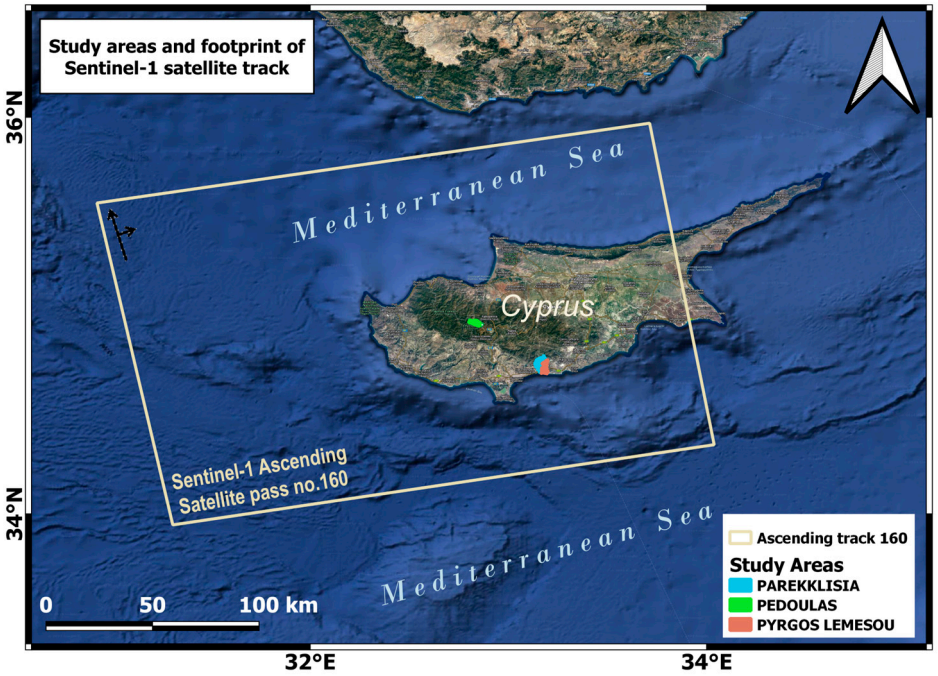

Figure 2. Study areas in Cyprus and the footprint of the Sentinel-1 images of ascending satellite pass 160 covering Cyprus and employed in the PSI analysis.

Table 1. Information about the Sentinel-1 SAR data for PSI analysis in the study areas.

Satellite Sensor	Satellite Pass	Time Period		No. of SLCs	Primary Image
Sentinel-1	160	20 February 2016	20 December 2021	136	10 June 2019

3.2. Methods

To investigate ground deformation phenomena in Pedoulas, Pyrgos and Parekklisia villages, remote sensing techniques validated via ground truth investigations and monthly precipitation data were employed. Specifically, multi-temporal InSAR was implemented on Sentinel-1 images to extract LOS surface displacements. Since SAR measurements refer to a direction towards or away from the satellite, to better interpret surface motion, further investigation of LOS displacements is required. Therefore, LOS displacements were projected to vertical surface displacements, using Equation (1)

$$v_{vert} = \frac{v_{LOS}}{\cos(\theta)} \quad (1)$$

where for each permanent scatterer v_{vert} represents the vertical displacement, v_{LOS} the LOS displacement and θ the incidence angle. The incidence angle is formed between the radar beam and the perpendicular to the Earth's surface, where the permanent scatterer is located.

The locations of ground truth investigations were mapped along with the results of the Persistent Scatterers Interferometry analysis. The deforming permanent scatterers nearby or on the identified deforming constructions were selected for further analysis. Time-series plots of annual precipitation data were generated along with time-series plots of vertical surface displacements. Finally, a correlation of the highest cumulative precipitation with

the initiation and progress of surface deformation phenomena in the investigated areas was performed. Figure 3 provides a detailed workflow of the methodology followed.

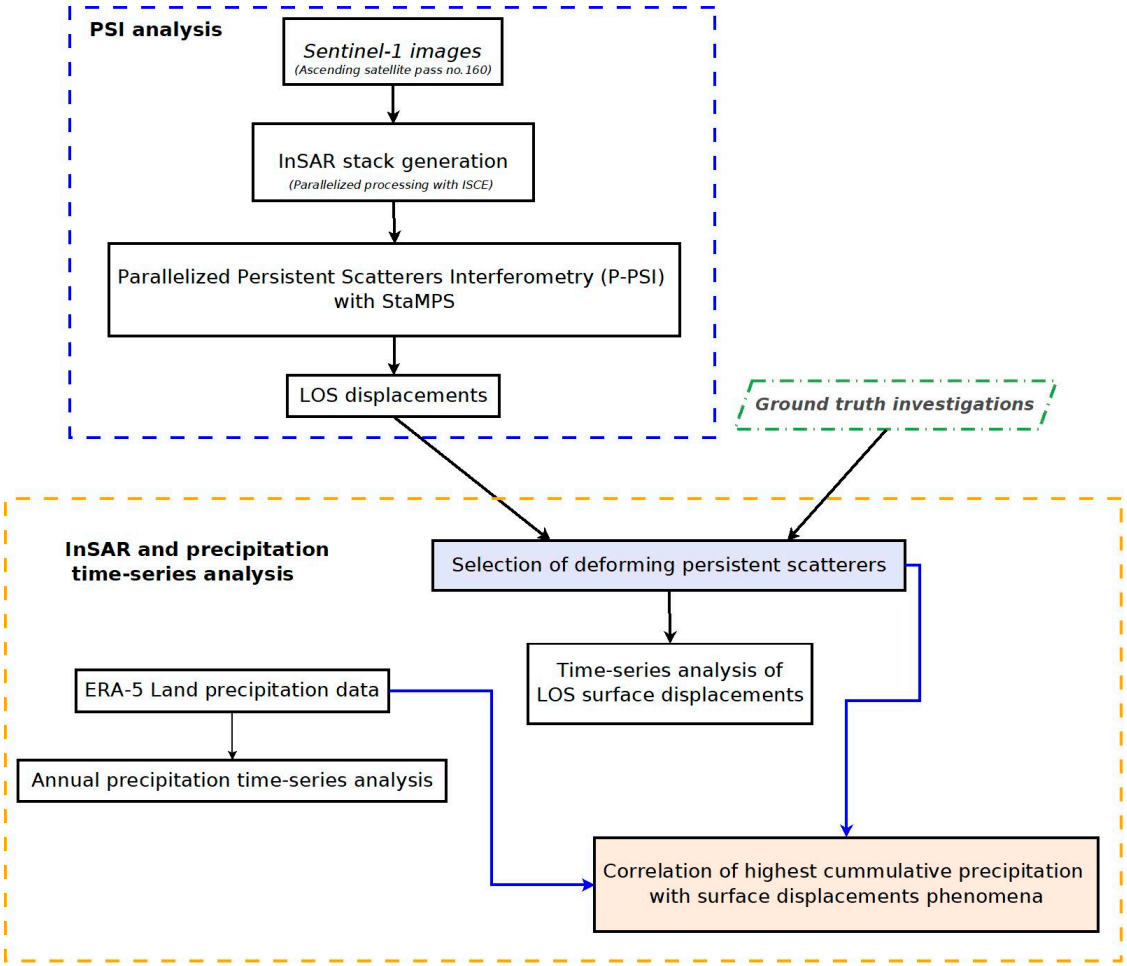

Figure 3. Workflow of the methodology followed.

Persistent Scatterers Interferometry

The large amount of Earth observation (EO) data dictates the need for faster and more efficient processing. The global coverage of Sentinel-1 sensor combined with the short revisit time, provides a rich archive of satellite data, tailored for monitoring timeless slow-moving deformation phenomena. Despite the unique advantages that the plethora of SAR data provides for geohazards monitoring, the exploitation of big volumes of Sentinel-1 data comprises several challenges. Sufficient storage and computational efficiency are some of the aspects that need to be seriously taken into consideration for PSI processing. A typical InSAR time-series analysis can be particularly time-consuming, especially, when analysing many years of surface deformation. Another serious aspect is the computational time that can be seriously increased when processing large volumes of Earth observation data.

In an attempt to manage the demands of big data geohazards monitoring, processing chains, services and tools have been developed to support the users and promote geohazards applications using big EO data. Furthermore, interventions in existing algorithms were performed to minimise the processing time. Some typical examples are the parallel small baseline subset (P-SBAS) processing chain [52–54], LiCSBAS [55–57], a tool for multi-temporal SAR interferometry with big volumes of Sentinel-1 data and SNAPPING [58], a surface displacements mapping tool using Sentinel-1 data that operates on the GEP platform. Finally, the European Ground Motion Service (EGMS) [59,60] provides a unique product of InSAR ground displacements in Europe with Sentinel-1 data.

Similarly, the Operational Unit, BEYOND Center for Earth Observation Research and Satellite Remote Sensing of the Institute for Astronomy, Astrophysics, Space Applications and Remote Sensing (IAASARS) of the National Observatory of Athens (NOA), developed an automated parallelised processing chain for PSI analysis of multi-sensor SAR data. InSAR time-series analysis was implemented on Sentinel-1 images covering the island of Cyprus with the parallelised PSI (P-PSI) processing chain [61]. The P-PSI is a parallelised version of the Stanford method for Persistent Scatterers Interferometry (PSI) [20] for the estimation of LOS displacements using big volumes of multi-sensor SAR satellite data, e.g., Sentinel-1, ERS, ENVISAT, TerraSAR-X, COSMO-SkyMed and ALOS data. The generation of the interferometric stack was performed with ISCE software [50,51]. The PSI was applied with StaMPS v4 software [62]. The P-PSI performed algorithmic interventions in both ISCE and StaMPS to speed-up the total process time. The LOS displacements were calibrated for atmospheric contributions that may affect the quality of the final SAR product using the open-source Toolbox for Reducing Atmospheric InSAR Noise (TRAIN) [63].

4. Results

4.1. LOS and Vertical Surface Displacements

The estimated LOS displacements in Pyrgos and Parekklisia villages revealed 5785 distinct locations on the ground, some of them related to noticeable ground deformation phenomena and others indicating surface stability. Similarly, 341 permanent scatterers were identified in Pedoulas village. Figure 4 presents LOS displacements for the affected areas as estimated with the P-PSI processing chain of the BEYOND centre (NOA, IAASARS).

By analysing the LOS displacements in Pedoulas village, negative displacements of a maximum rate of -10 mm/y are presented. The deforming scatterers with the maximum velocity rates were identified to the southwest and east of the village, while negative velocities of a smaller scale were also identified all over the village. In Pyrgos and Parekklisia villages, the LOS displacements presented positive displacements with a maximum rate of 8 mm/y.

To project the LOS signals observed in Pedoulas, Pyrgos and Parekklisia villages, vertical displacements were calculated by dividing the LOS velocity with the cosine of the look angle value of each scatterer. Figure 5 presents the vertical components of LOS ground motion in the deforming villages.

Evaluating the above-described spatial distribution of the deformations, in Figure 6a, areas A and B seemed to indicate that the heads of two shallow landslides were active at the higher SW parts of the village, while in area C, the head of a third landslide was at the lower NE part of the village. The first two landslides are also presented in the 3D view of Pedoulas village in Figure 6b, and affected the core of the village, while the third extended downhill towards the base of the cleft bearing the village. These landslide movements can cause nearly the entire village to slide with various velocities. In Figure 6c, lower displacements and positive deformation rates were identified in Parekklisia, which increased while moving closer to Pyrgos village, thus forming two contours of vertical displacements in Pyrgos-Parekklisia areas.

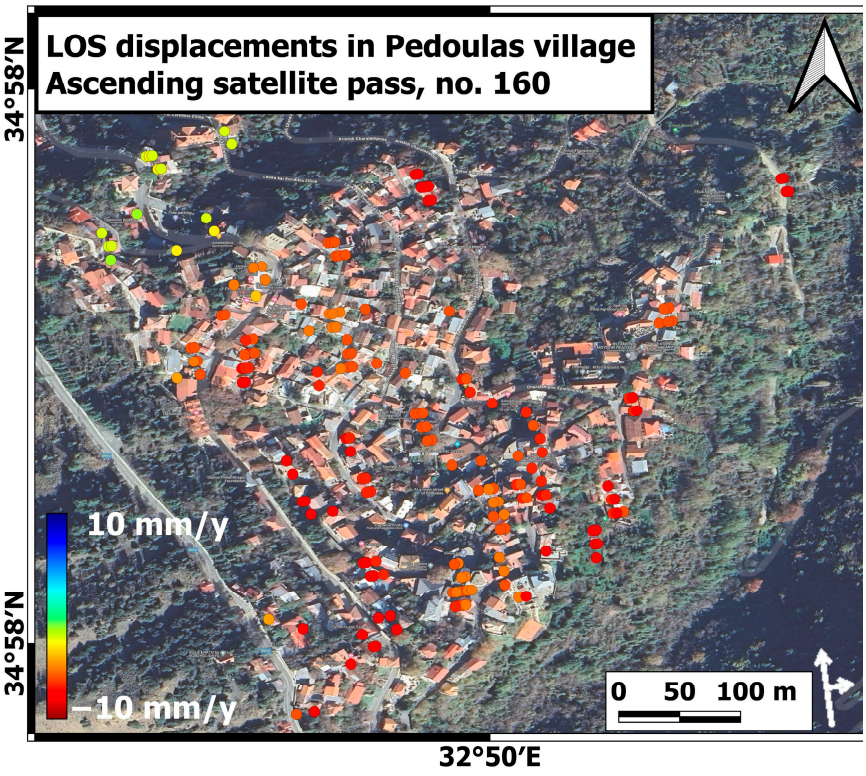

(**a**)

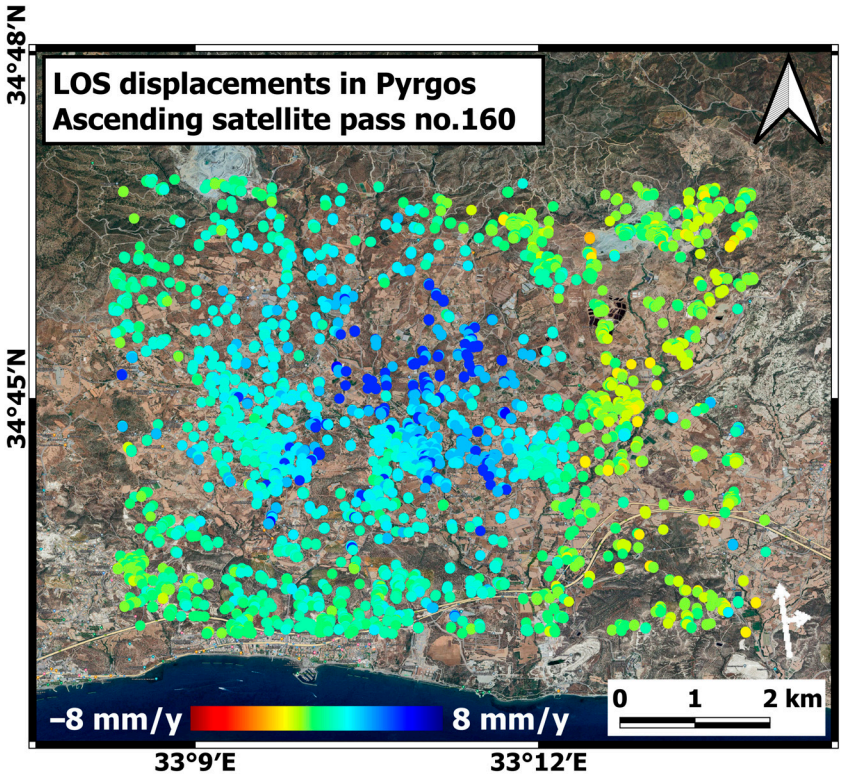

(**b**)

Figure 4. LOS displacements from the ascending satellite pass of Sentinel-1 sensor for (**a**) Pedoulas and (**b**) Pyrgos-Parekklisia deforming sites in Cyprus.

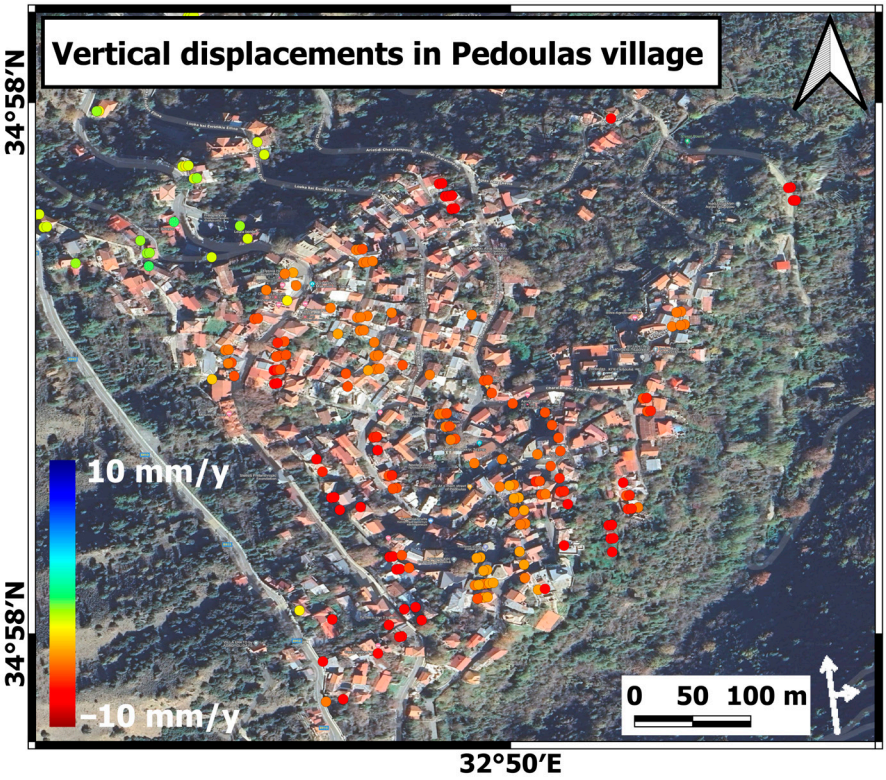

(**a**)

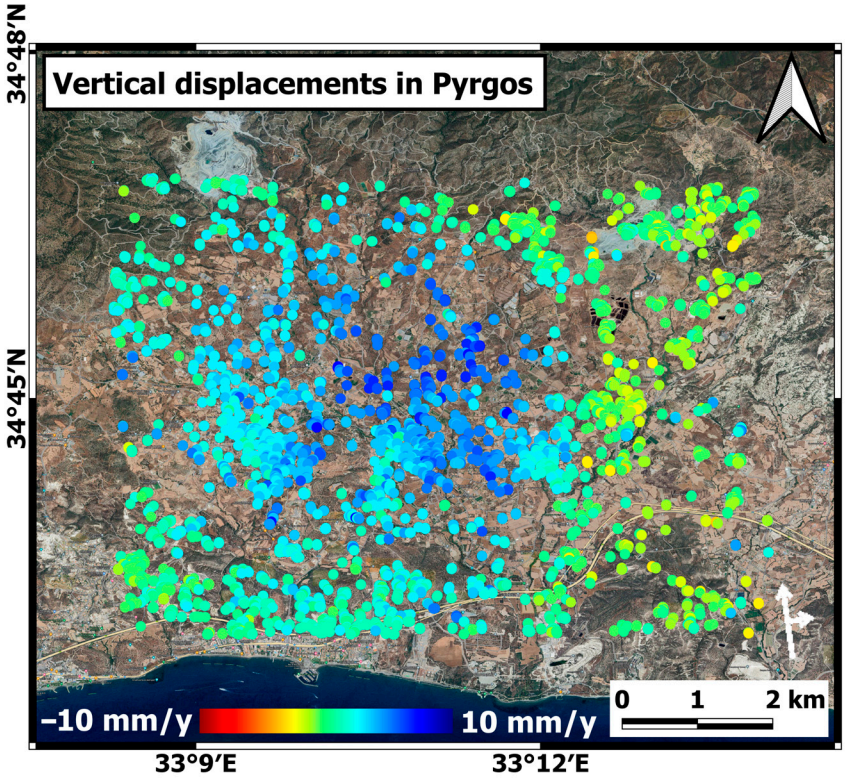

(**b**)

Figure 5. Vertical displacements estimated from Sentinel-1 LOS displacements for (**a**) Pedoulas village and (**b**) Pyrgos-Parekklisia villages in Cyprus.

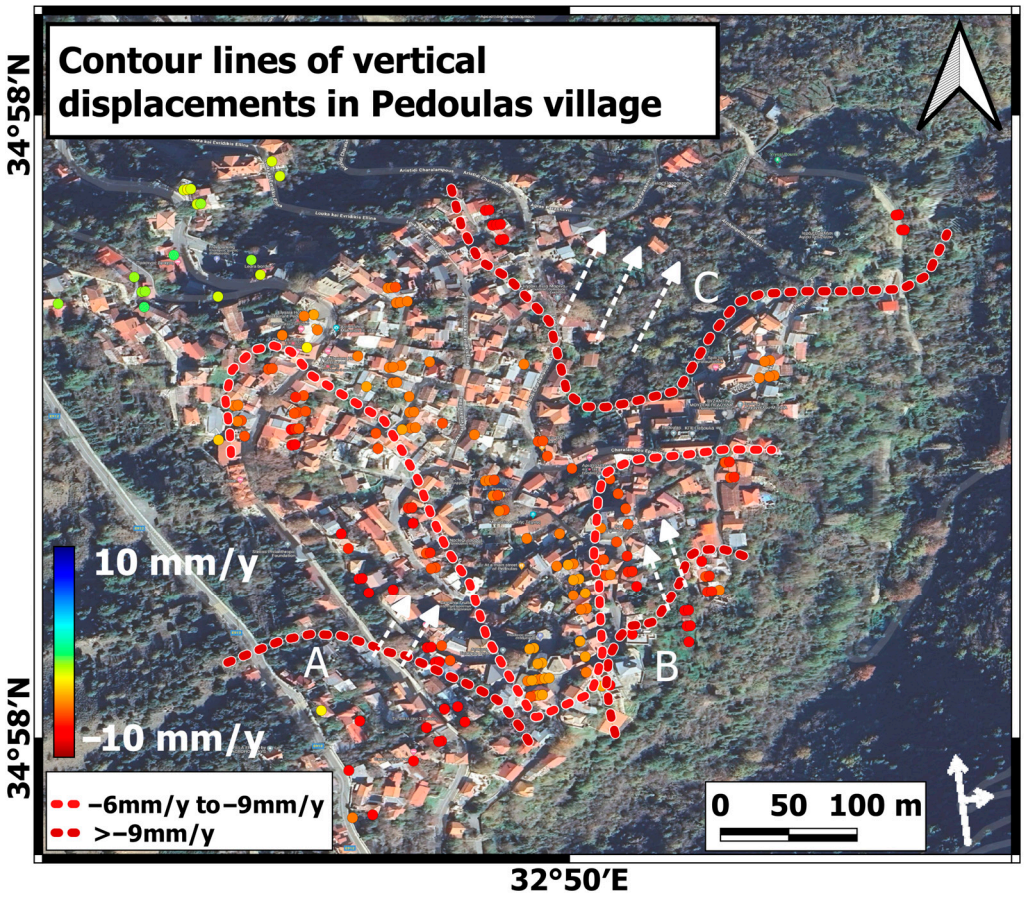

(**a**)

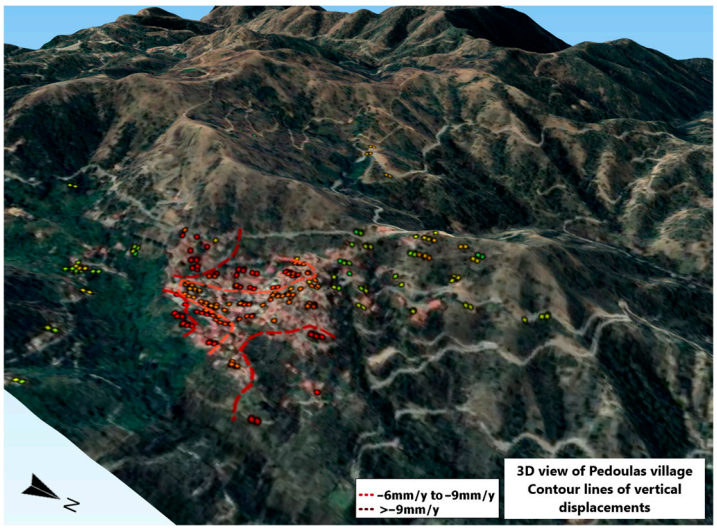

(**b**)

Figure 6. *Cont.*

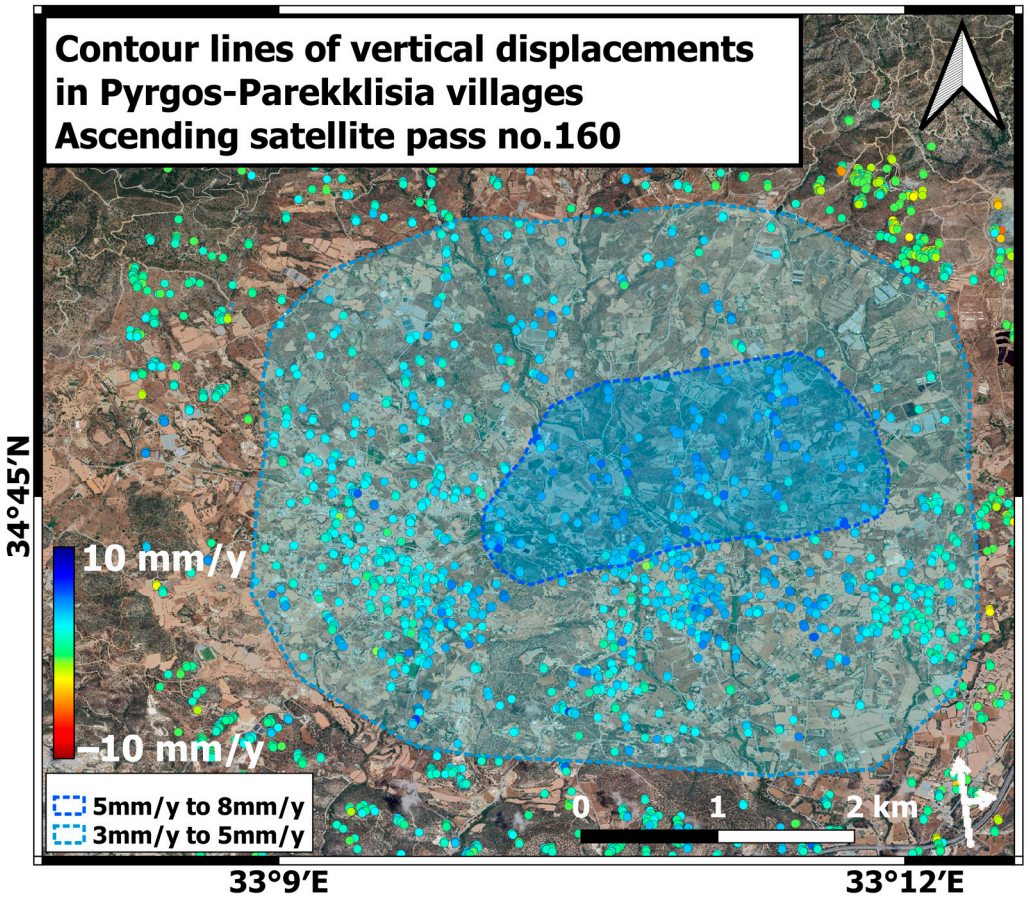

(**c**)

Figure 6. Contours based on the variations of vertical InSAR displacements of the ascending satellite pass (**a**) for Pedoulas village (**b**) for Pedoulas village with a 3D view and (**c**) Pyrgos-Parekklisia villages in Cyprus. In Figure (**a**), white arrows depict the orientation of movement of the existing landslide.

4.2. Ground Truth Investigations

The observed InSAR time-series analysis results, were validated via ground truth observations in the affected areas. Field visits were performed in Pedoulas and Pyrgos-Parekklisia allowing damage to be identified. Although extensive damage was recorded in both case studies, only the damage to buildings that coincided with deforming PS scatterers were included in the present manuscript. For this purpose, in each mapped deforming site, an identification of PSI points that were either situated on the same deforming constructions or in the narrow area around the deforming construction was performed. The locations of ground truth observations and the closer identified PS points are presented in Figure 7. To select the PS scatterers that corresponded to ground truth observations, extended photointerpretation was performed in a GIS environment to identify the buildings that presented evidence of surface deformation based on the location of the ground truth observations. Similarly, the scatterers located on these buildings were eliminated from the initial PSI analysis for further investigation. An additional analysis of the kinematic behaviour of the scatterers coinciding with ground truth observations was performed to investigate and define the driving mechanisms of the observed ground deformation phenomena.

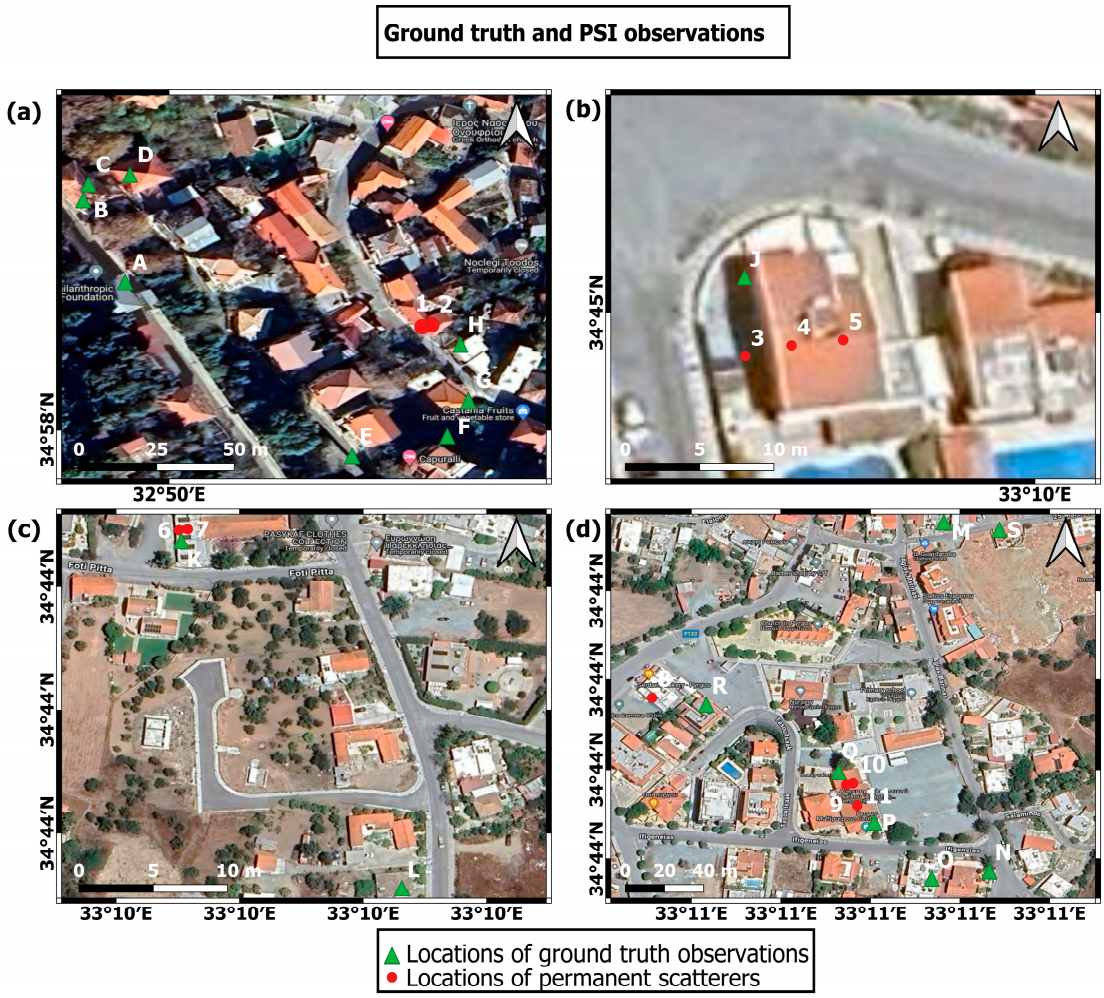

Figure 7. Locations of ground truth observations and PSI of ascending Sentinel-1 satellite pass in (**a**) Pedoulas village, (**b**) Pyrgos village, (**c**) and (**d**) Parekklisia village in Cyprus. Capital letters present the locations of ground truth observations. Red numbers indicate the permanent scatterers, located on the deforming constructions or in the narrow area around the deforming constructions.

Ground truth observations, including typical examples of deformation on construction sites, are induced by landslides and swelling/shrinking phenomena. In the present study, indicative examples are presented along with time-series analysis of the closer to the affected construction PS points. Figure 8 presents indicative examples of deformation in the areas of interest that are depicted and marked with red arrows.

LOS displacements provide evidence of ground deformation phenomena and the spatial sampling of PSs gives insights into the deformation mechanism. However, the interpretation of surface deformation phenomena requires additional observations. In the absence of geodetic measurements, field observations in Pedoulas, Pyrgos and Parekklisia villages provided a unique advantage to validate the identified InSAR displacements.

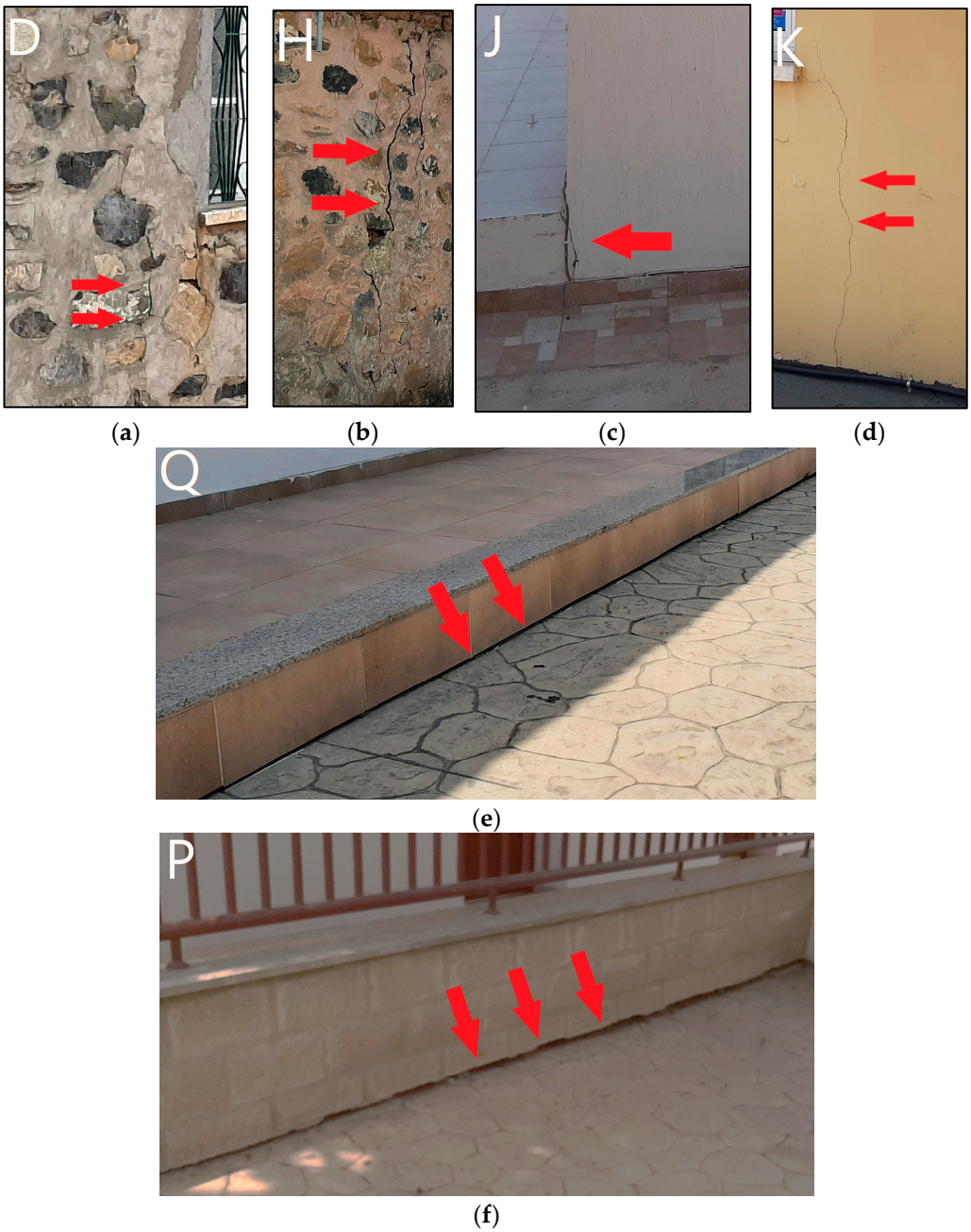

Figure 8. Observed deformation in constructions in (**a**,**b**) Pedoulas and (**c**–**f**) Pyrgos-Parekklisia villages in Cyprus. At the top left of each image, the letter of the ground truth observation at each site, as presented in Figure 7, is added. Red arrows depict areas with differential displacements.

5. Discussion

InSAR analysis, validated via ground truth investigations, revealed rainfall-induced surface displacements in Pedoulas and Pyrgos-Parekklisia villages. To further investigate the impact of precipitation on the observed ground deformation phenomena, time-series analysis of vertical displacements and precipitation data was conducted. Time-series plots from 2017 to 2021 were generated from the vertical displacements of the selected scatterers situated on the deforming constructions. LOS displacements from 2016 were excluded from the time-series analysis plots due to the absence of an adequate number of observations before 2017; therefore, the addition of 2016 would lead to a large gap in the time-series plots and misinterpreted conclusions.

Swelling/shrinking phenomena or subsidence due to the overexploitation of the aquifers cannot be excluded from the deformation mechanisms due to the geomorphology of the affected areas. However, for a better interpretation of the surface deformation phenomena and in the absence of previous related research on the specific AOIs, the possible correlation of surface displacements with high precipitation rates was also investigated. Many studies have been conducted to analyse the correlation between rainfall and surface deformation phenomena. A time-series analysis of InSAR and precipitation data [64–66] is usually performed to investigate the existence of a correlation between extreme rainfall and surface deformation phenomena. Furthermore, Liu et al. [67] proposed a wavelet analysis for assessing the quantitative relationship between precipitation and landslides.

In Pedoulas and Pyrgos-Parekklisia villages, precipitation time-series analysis from 2017 to 2021 was performed, using an ERA-5 Land [47] hourly precipitation re-analysis dataset. Since two images per month of Sentinel-1 data were employed in the InSAR time-series analysis, in order to correlate the precipitation rates with the InSAR vertical surface displacements, the total maximum monthly precipitation rate was estimated and plotted along with InSAR vertical surface displacements. To assist the data processing, linear time series interpolation was applied to assign a ground displacement value on the precipitation dates at the end of each month. Furthermore, for each of the PS time series, the months with the minimum and the maximum precipitation during the summer and the winter respectively were identified. Between successive minimum-maximum and maximum-minimum month pairs for each year, trend lines for the displacement values were calculated via the least squares polynomial fit method and plotted.

By analysing the time-series plots in Figures 9 and 10, a pattern can be observed. As expected, the highest precipitation rates were recorded during the winter months between December and until March of the next year, while during the summer months, precipitation rates were low to zero.

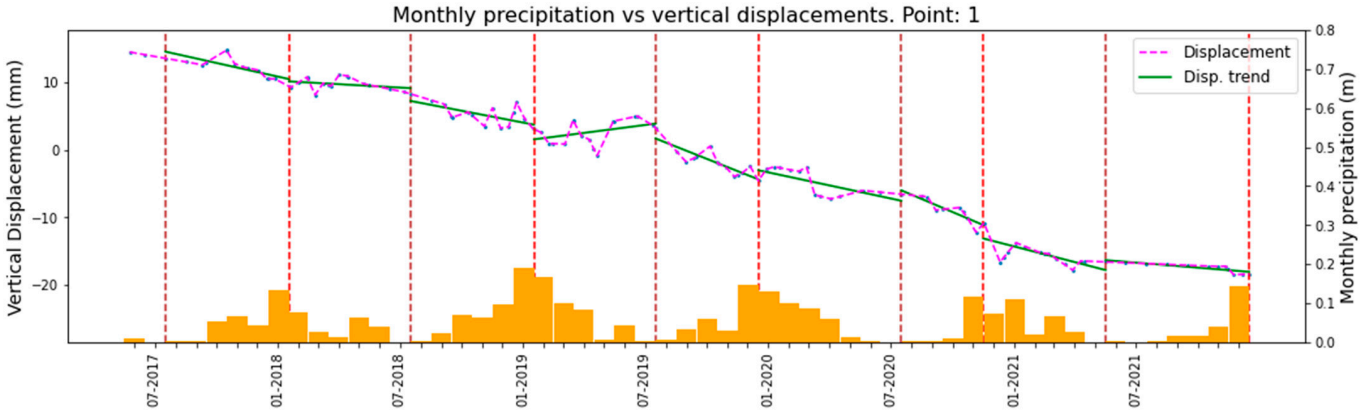

Figure 9. Vertical InSAR displacements along with precipitation rates for PS point no.1 in Pedoulas village in Cyprus. Red vertical dashed lines represent the maximum precipitation rates while brown vertical dashed lines represent the minimum precipitation rates.

For the investigation of the phenomena taking place at Pedoulas village, the vertical deformation rates were correlated with the precipitation rates. As presented in the time-series plot of the permanent scatterer no. 1 (Figure 9) and identified in Pedoulas village (Figure 7a), the deformation rates appeared to be stable during the rainy season while increasing during the summer.

For the Pyrgos-Parekklisia villages, Figure 10 shows the time-series plots for selected scatterers indicating that uplifting vertical displacements start to increase when precipitation reaches the maximum values and continue evolving during the summer until the formations dry out.

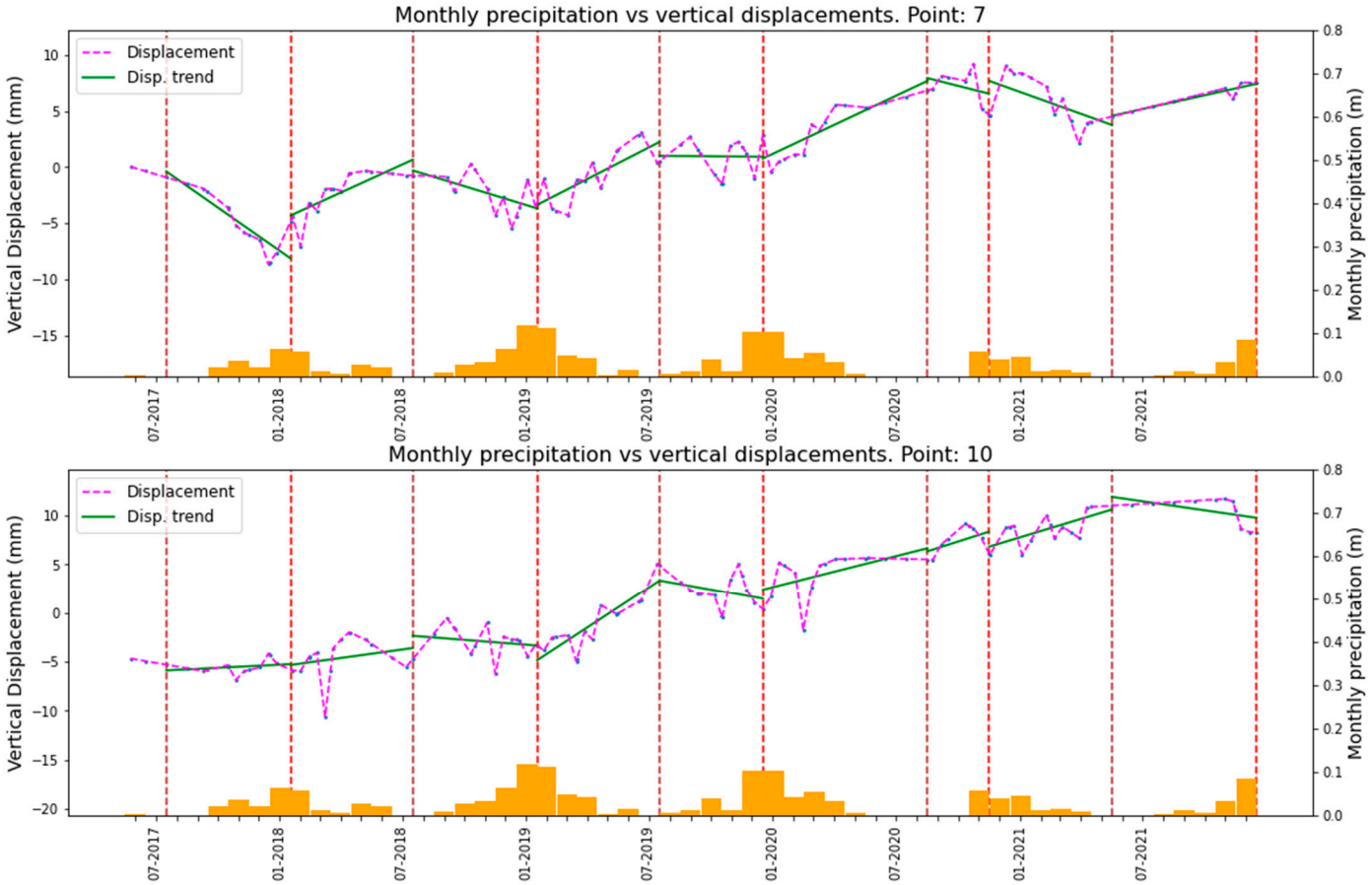

Figure 10. Vertical InSAR displacements along with precipitation rates for selected PS points in Pyrgos-Parekklisia villages in Cyprus. Red vertical dashed lines represent the maximum precipitation rates while brown vertical dashed lines represent the minimum precipitation rates.

Aiming to provide a generalised conclusion about the deformation regime of the study areas in Cyprus and the impact of high precipitation rates in the existing deformation, additional analysis of the vertical displacements and precipitation rates was conducted. A correlation of the highest cumulative annual precipitation with the initiation and the extent of ground deformation phenomena was conducted. By using the identified minimum and maximum precipitation months, the accumulated precipitation and accumulated deformation from each one of the summer minimum precipitation months through the following year's summer minimum were calculated. Similar to the plots in Figures 9 and 10, between successive minimum-maximum and maximum-minimum month pairs for each year, trend lines for the accumulated displacement are plotted.

In accordance to the results acquired from the correlation of the deformation and precipitation rates (Figure 9), the accumulated precipitation at the Pedoulas village during winter (Figure 11) did not affect the accumulated deformation rate. Therefore, the winter rains were not enough to speed up the landslide movements, which keep moving at a steady rate. On the contrary, the increase in the deformations during the spring and summer can be justified by the fact that during these months, the population of the village steadily increases as most of the houses operate as cottages. The lack of a sewerage system and the use of absolving pits increase the ground water level, speeding up the landslide movements.

Respectively, in accordance to the results acquired from the correlation of the deformation and precipitation rates (Figure 10), the accumulated precipitation at the Pyrgos-Parekklisia villages during the winter (Figure 12) started to increase the uplifting deformation since the middle of the winter (December–January). As witnessed in Figures 10 and 12, the uplifting phenomena stop evolving when the formations dry out during the summer.

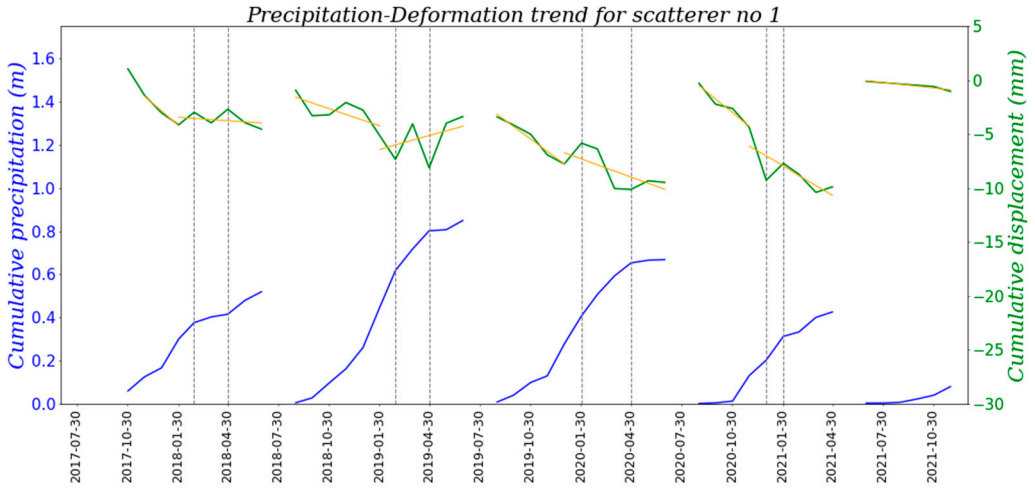

Figure 11. Plot of cumulative vertical displacements and cumulative precipitation rates for scatterer 1 in Pedoulas village in Cyprus. The grey dashed vertical lines represent the beginning and the end of the increase in precipitation.

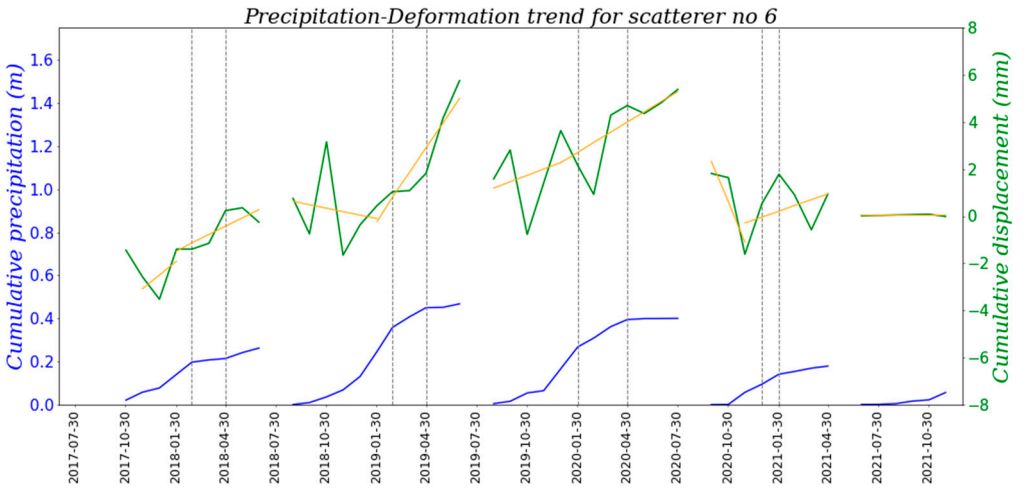

Figure 12. Plot of cumulative vertical displacements and cumulative precipitation rates for scatterer 6 in Pyrgos village in Cyprus. The grey dashed vertical lines represent the beginning and the end of the increase in precipitation.

6. Conclusions

As a result of our research, we have established that Pedoulas and Pyrgos-Parekklisia villages in Cyprus are exposed to rainfall-induced surface deformation phenomena. The estimated LOS and vertical displacements revealed negative vertical movements in Pedoulas village, with maximum displacement rates of −10 mm/y due to landslide phenomena. Furthermore, positive surface displacements were identified in Pyrgos-Parekklisia villages attributed to the swelling phenomena. The estimated LOS displacements were validated via ground truth observations that presented characteristic deformation in buildings at all three sites. A precipitation analysis from 2017 to 2021 provided data to examine the correlation between surface displacement rates and intense precipitation events, especially during the winter months. The analysis showed that at the Pedoulas village, the landslide movements were most intensively affected during the spring and summer months where the village receives many tourists yet, due to the lack of sewerage system, there is an infiltration of waste water in the ground, rather than from the increased precipitation during the winter. At the Pyrgos-Parekklisia villages, it was shown that there is a time lag between the beginning of the rain season and the start of the swelling phenomena as the moisture of

the ground formations takes time to accumulate, as suggested by the swelling phenomena that takes place between December and January.

InSAR results, validated via ground truth observations and a precipitation analysis, proved to be very efficient in the identification of the driving mechanisms of surface deformation phenomena in Pedoulas and Pyrgos-Parekklisia villages. The knowledge of the deformation regime, not only in the specific villages, but also in additional areas in Cyprus with similar ground displacement trends, will contribute to their proper mitigation and prevention. In future work, the further investigation of the identified displacements with additional remote sensing techniques as well as ground-based methods will complement and support the findings of the present study and highlight the efficiency of multidisciplinary and complementary methods for mapping and monitoring various ground displacement phenomena.

Author Contributions: Conceptualisation, S.A., C.K. and C.L.; methodology, S.A. and C.L.; validation, C.L. and C.K.; formal analysis, S.A. and A.A.; investigation, S.A. and C.L.; resources, C.K. and C.D.; data curation, S.A. and A.A.; writing—original draft preparation, S.A., C.L. and A.A.; writing—review and editing, S.A., C.L., M.T., A.A., C.K., C.D., K.T. and D.G.H.; visualisation, S.A. and A.A.; supervision, C.L. and C.K.; project administration, C.K. and D.G.H. All authors have read and agreed to the published version of the manuscript.

Funding: This work was funded through the EXCELSIOR Teaming project (Grant Agreement No. 857510, www.excelsior2020.eu, accessed on 7 December 2023) that has received funding from the European Union's Horizon 2020 research and innovation programme and from the Government of the Republic of Cyprus through the Directorate General for the European Programmes, Coordination and Development.

Data Availability Statement: The data presented in this study are available on request from the corresponding author.

Acknowledgments: The authors acknowledge the 'EXCELSIOR': ERATOSTHENES: Excellence Research Centre for Earth Surveillance and Space-Based Monitoring of the Environment H2020 Widespread Teaming project (www.excelsior2020.eu, accessed on 7 December 2023). The 'EXCELSIOR' project has received funding from the European Union's Horizon 2020 research and innovation programme under Grant Agreement No 857510, from the Government of the Republic of Cyprus through the Directorate General for the European Programmes, Coordination and Development and the Cyprus University of Technology.

Conflicts of Interest: The authors declare no conflicts of interest. The funders had no role in the design of the study; in the collection, analyses, or interpretation of data; in the writing of the manuscript; or in the decision to publish the results.

References

1. Wilde, M.; Günther, A.; Reichenbach, P.; Malet, J.-P.; Hervás, J. Pan-European landslide susceptibility mapping: ELSUS Version 2. *J. Maps* **2018**, *14*, 97–104. [CrossRef]
2. Alexakis, D.D.; Agapiou, A.; Tzouvaras, M.; Themistocleous, K.; Neocleous, K.; Michaelides, S.; Hadjimitsis, D.G. Integrated use of GIS and remote sensing for monitoring landslides in transportation pavements: The case study of Paphos area in Cyprus. *Nat. Hazards* **2014**, *72*, 119–141. [CrossRef]
3. Efthymiou, M.; Hadjicharalambous, K.L. *Landslides in Cyprus and Their Consequences to the Built Environment*; Geological Survey Department of the Republic of Cyprus: Strovolos, Cyprus, 2013.
4. Eyre, T.S.; Samsonov, S.; Feng, W.; Kao, H.; Eaton, D.W. InSAR data reveal that the largest hydraulic fracturing-induced earthquake in Canada, to date, is a slow-slip event. *Sci. Rep.* **2022**, *12*, 2043. [CrossRef]
5. Pieraccini, M.; Mecatti, D.; Noferini, L.; Luzi, G.; Franchioni, G.; Atzeni, C. SAR interferometry for detecting the effects of earthquakes on buildings. *NDT E Int.* **2002**, *35*, 615–625. [CrossRef]
6. Serkhane, A.; Benfedda, A.; Guettouche, M.S.; Bouhadad, Y. InSAR derived co-seismic deformation triggered by the Mihoub (Tell Atlas of Algeria) 28 May 2016 (Mw = 5.4) earthquake combined to geomorphic features analysis to identify the causative active fault. *J. Afr. Earth Sci.* **2022**, *188*, 104476. [CrossRef]
7. Kontoes, C.; Alatza, S.; Chousianitis, K.; Svigkas, N.; Loupasakis, C.; Atzori, S.; Apostolakis, A. Coseismic Surface Deformation, Fault Modeling, and Coulomb Stress Changes of the March 2021 Thessaly, Greece, Earthquake Sequence Based on InSAR and GPS Data. *Seismol. Res. Lett.* **2022**, *93*, 2584–2598. [CrossRef]

8. Wang, T.; Zhu, S.N.; Yang, C.S.; Wei, Y.J.; Zhao, C.Y.; Hou, H.C. Co- and Post-seismic Deformation Mechanisms of the 2020 Mw6.0 Jiashi Earthquake in Xinjiang (China), Revealed by Sentinel-1 InSAR Observations. *Front. Environ. Sci.* **2022**, *10*, 933200. [CrossRef]
9. Liu, F.; Elliott, J.R.; Craig, T.J.; Hooper, A.; Wright, T.J. Improving the resolving power of InSAR for earthquakes using time series: A case study in Iran. *Geophys. Res. Lett.* **2021**, *48*, e2021GL093043. [CrossRef]
10. Dawson, J.; Cummins, P.; Tregoning, P.; Leonard, M. Shallow intraplate earthquakes in Western Australia observed by Interferometric Synthetic Aperture Radar. *J. Geophys. Res.* **2008**, *113*, B11408. [CrossRef]
11. Li, Y.; Jiang, W.; Zhang, J.; Li, B.; Yan, R.; Wang, X. Sentinel-1 SAR-Based coseismic deformation monitoring service for rapid geodetic imaging of global earthquakes. *Nat. Hazards Res.* **2021**, *1*, 11–19. [CrossRef]
12. Pritchard, M.; Biggs, J.; Wauthier, C.; Sansosti, E.; Arnold, D.W.D.; Delgado, F.; Ebmeier, S.K.; Henderson, S.T.; Stephens, K.; Cooper, C.; et al. Towards coordinated regional multi-satellite InSAR volcano observations: Results from the Latin America pilot project. *J. Appl. Volcanol.* **2018**, *7*, 5. [CrossRef]
13. Garthwaite, M.C.; Miller, V.L.; Saunders, S.; Parks, M.M.; Hu, G.; Parker, A.L. A Simplified Approach to Operational InSAR Monitoring of Volcano Deformation in Low- and Middle-Income Countries: Case Study of Rabaul Caldera, Papua New Guinea. *Front. Earth Sci.* **2019**, *6*, 240. [CrossRef]
14. Hooper, A.; Wright, T.J.; Weiss, J.R.; Rollins, C.; Gaddes, M.; Lazecky, M.; Morishita, Y.; Walters, R.J.; Wang, H.; Hussain, E. Exploiting InSAR on a Large Scale for Tectonics and Volcano Monitoring. In Proceedings of the IGARSS 2020–2020 IEEE International Geoscience and Remote Sensing Symposium, Waikoloa, HI, USA, 26 September–2 October2020; pp. 6857–6858. [CrossRef]
15. Joughin, I.; Smith, B.; Abdalati, W. Glaciological advances made with interferometric synthetic aperture radar. *J. Glaciol.* **2010**, *56*, 1026–1042. [CrossRef]
16. Wempen, J. Application of DInSAR for short period monitoring of initial subsidence due to longwall mining in the mountain west United States. *Int. J. Min. Sci. Technol.* **2020**, *30*, 33–37. [CrossRef]
17. Fan, H.; Lian, X.; Yang, W.; Ge, L.; Hu, H.; Du, Z. Mining large-gradient subsidence monitoring using D-InSAR optimized by GNSS. *Imaging Sci. J.* **2021**, *69*, 207–218. [CrossRef]
18. Achache, J.; Fruneau, B.; Delacourt, C. Applicability of SAR Interferometry for Monitoring of Landslides. In Proceedings of the Second ERS Applications Workshop, London, UK, 6–8 December 1995. (ESA SP-383, February 1996).
19. Ferretti, A.; Prati, C.; Rocca, F. Permanent scatterers in SAR interferometry. *IEEE Trans. Geosci. Remote Sens.* **2001**, *39*, 8–20. [CrossRef]
20. Hooper, A.; Zebker, H.; Segall, P.; Kampes, B. A new method for measuring deformation on volcanoes and other natural terrains using InSAR persistent scatterers. *Geophys. Res. Lett.* **2004**, *31*, 1–5. [CrossRef]
21. Kampes, B. *Radar Interferometry-Persistent Scatterer Technique*; Springer: Dordrecht, The Netherlands, 2006; Volume 12. [CrossRef]
22. Berardino, P.; Fornaro, G.; Lanari, R.; Sansosti, E. A new algorithm for surface deformation monitoring based on small baseline differential SAR interferograms. *Geosci. Remote Sens. IEEE Trans.* **2002**, *40*, 2375–2383. [CrossRef]
23. Lanari, R.; Mora, O.; Manunta, M.; Mallorquí, J.; Berardino, P.; Sansosti, E. A small-baseline approach for investigating deformations on full-resolution differential SAR interferograms. *Geosci. Remote Sens. IEEE Trans.* **2004**, *42*, 1377–1386. [CrossRef]
24. Bekaert, D.; Handwerger, A.; Agram, P.; Kirschbaum, D. InSAR-based detection method for mapping and monitoring slow-moving landslides in remote regions with steep and mountainous terrain: An application to Nepal. *Remote Sens. Environ.* **2020**, *249*, 111983. [CrossRef]
25. Smail, T.; Abed, M.; Mebarki, A.; Lazecky, M. Earthquake-induced landslide monitoring and survey by means of InSAR. *Nat. Hazards Earth Syst. Sci.* **2022**, *22*, 1609–1625. [CrossRef]
26. Kang, Y.; Lu, Z.; Zhao, C.; Xu, Y.; Kim, J.; Gallegos, A. InSAR monitoring of creeping landslides in mountainous regions: A case study in Eldorado National Forest, California. *Remote Sens. Environ.* **2021**, *258*, 112400. [CrossRef]
27. Kulsoom, I.; Hua, W.; Hussain, S.; Chen, Q.; Khan, G.; Shihao, D. SBAS-InSAR based validated landslide susceptibility mapping along the Karakoram Highway: A case study of Gilgit-Baltistan, Pakistan. *Sci. Rep.* **2023**, *13*, 1–20. [CrossRef]
28. Pawluszek-Filipiak, K.; Borkowski, A.; Motagh, M. Multi-temporal landslide activity investigation by spaceborne SAR interferometry: The case study of the Polish Carpathians. *Sens. Appl. Soc. Environ.* **2021**, *24*, 100629. [CrossRef]
29. Hussain, S.; Pan, B.; Afzal, Z.; Ali, M.; Zhang, X.; Shi, X. Landslide detection and inventory updating using the time-series InSAR approach along the Karakoram Highway, Northern Pakistan. *Sci. Rep.* **2023**, *13*, 7485. [CrossRef]
30. Poland, M.P.; Zebker, H.A. Volcano geodesy using InSAR in 2020: The past and next decades. *Bull. Volcanol.* **2022**, *84*, 27. [CrossRef]
31. Spaans, K.; Hooper, A. InSAR processing for volcano monitoring and other near-real time applications. *J. Geophys. Res. Solid Earth* **2016**, *121*, 2947–2960. [CrossRef]
32. Joshi, M.; Kothyari, G.C.; Malik, K.; Taloor, A.K. Response of drainage to tectonics and PS-InSAR derived deformation study in Bilaspur, northwestern Himalaya, India. *Geod. Geodyn.* **2022**, *13*, 205–218. [CrossRef]
33. Alatza, S.; Papoutsis, I.; Paradissis, D.; Kontoes, C.; Papadopoulos, G.A.; Raptakis, C. InSAR Time-Series Analysis for Monitoring Ground Displacement Trends in the Western Hellenic Arc: The Kythira Island, Greece. *Geosciences* **2020**, *10*, 293. [CrossRef]

34. Antonielli, B.; Monserrat, O.; Bonini, M.; Cenni, N.; Devanthéry, N.; Righini, G.; Sani, F. Persistent Scatterer Interferometry analysis of ground deformation in the Po Plain (Piacenza-Reggio Emilia sector, Northern Italy): Seismo-tectonic implications. *Geophys. J. Int.* **2016**, *206*, 1440–1455. [CrossRef]
35. Huang, C.; Xia, H.; Hu, J. Surface Deformation Monitoring in Coal Mine Area Based on PSI. *IEEE Access* **2019**, *7*, 29672–29678. [CrossRef]
36. Aswathi, J.; Binoj Kumar, R.B.; Oommen, T.; Bouali, E.H.; Sajinkumar, K.S. InSAR as a tool for monitoring hydropower projects: A review. *Energy Geosci.* **2022**, *3*, 160–171. [CrossRef]
37. Alipour, S.; Motgah, M.; Sharifi, M.A.; Walter, T.R. InSAR time series investigation of land subsidence due to groundwater overexploitation in Tehran, Iran. In Proceedings of the 2008 Second Workshop on Use of Remote Sensing Techniques for Monitoring Volcanoes and Seismogenic Areas, Napoli, Italy, 11–14 November 2008; pp. 1–5. [CrossRef]
38. Bai, L.; Jiang, L.; Zhao, Y.; Li, Z.; Cao, G.; Zhao, C.; Liu, R.; Wang, H. Quantifying the influence of long-term overexploitation on deep groundwater resources across Cangzhou in the North China Plain using InSAR measurements. *J. Hydrol.* **2022**, *605*, 127368. [CrossRef]
39. Castellazzi, P.; Schmid, W. Interpreting C-band InSAR ground deformation data for large-scale groundwater management in Australia. *J. Hydrol. Reg. Stud.* **2021**, *34*, 100774. [CrossRef]
40. González-Jiménez, M.; Guardiola-Albert, C.; Ezquerro, P.; Aguilera, H.; Béjar-Pizarro, M.; Naranjo-Fernández, N.; Bru, G.; Herrera, G. Analysis of aquifer-system deformation in the Doñana Natural Space (Spain) using unsupervised cloud-computed InSAR data and wavelet analysis. *Water Resour. Res.* **2023**, *59*, e2022WR033858. [CrossRef]
41. Ali, M.Z.; Chu, H.-J.; Tatas; Burbey, T.J. Estimation of annual groundwater changes from InSAR-derived land subsidence. *Water Environ. J.* **2022**, *36*, 622–632. [CrossRef]
42. Kaitantzian, A.; Loupasakis, C.; Tzampoglou, P.; Parcharidis, I. Ground Subsidence Triggered by the Overexploitation of Aquifers Affecting Urban Sites: The Case of Athens Coastal Zone along Faliro Bay (Greece) Hindawi. *Geofluids* **2020**, *2020*, 8896907. [CrossRef]
43. Antoniadis, N.; Alatza, S.; Loupasakis, C.; Kontoes, C. Land Subsidence Phenomena vs. Coastal Flood Hazard—The Cases of Messolonghi and Aitolikon (Greece). *Remote Sens.* **2023**, *15*, 2112. [CrossRef]
44. Agapiou, A.; Lysandrou, V. Detecting Displacements Within Archaeological Sites in Cyprus After a 5.6 Magnitude Scale Earthquake Event Through the Hybrid Pluggable Processing Pipeline (HyP3) Cloud-Based System and Sentinel-1 Interferometric Synthetic Aperture Radar (InSAR) Analysis. *IEEE J. Sel. Top. Appl. Earth Obs. Remote Sens.* **2020**, *13*, 6115–6123. [CrossRef]
45. Michalis, P.; Giourou, A.; Charalampopoulou, B.; Li, Z.; Li, Y. Land subsidence in southwest Cyprus revealed from C-band radar interferometry. In Proceedings of the Second International Conference on Remote Sensing and Geoinformation of the Environment (RSCy2014), Paphos, Cyprus, 7–10 April 2014; p. 9229. [CrossRef]
46. Danezis, C.; Kakoullis, D.; Fotiou, K.; Pekri, M.; Chatzinikos, M.; Kotsakis, C.; Brcic, R.; Eineder, M.; Nikolaidis, M.; Ioannou, G.; et al. CyCLOPS: A National Integrated GNSS/InSAR Strategic Research Infrastructure for Monitoring Geohazards and Forming the Next Generation Datum of the Republic of Cyprus. In *International Association of Geodesy Symposia*; Springer: Berlin/Heidelberg, Germany, 2022. [CrossRef]
47. Muñoz Sabater, J. ERA5-Land Hourly Data from 1950 to Present. Copernicus Climate Change Service (C3S) Climate Data Store (CDS). 2019. Available online: https://cds.climate.copernicus.eu/cdsapp#!/dataset/10.24381/cds.e2161bac?tab=overview (accessed on 7 December 2023).
48. George, R.P. Structural petrology of the Olympus ultramafic complex in the Troodos ophiolite, Cyprus. *Geol. Soc. Am. Bull.* **1978**, *89*, 845–865. [CrossRef]
49. Abelson, M.; Baer, G.; Agnon, A. Evidence from gabbro of the Troodos ophiolite for lateral magma transport along a slow-spreading mid-ocean ridge. *Nature* **2001**, *409*, 72–75. [CrossRef]
50. Rosen, P.A.; Gurrola, E.; Sacco, G.F.; Zebker, H. The InSAR scientific computing environment. In Proceedings of the EUSAR 2012 9th European Conference on Synthetic Aperture Radar, Nuremberg, Germany, 23–26 April 2012.
51. Fattahi, H.; Agram, P.; Simons, M. A network-based enhanced spectral diversity approach for TOPS Time-Series Analysis. *IEEE Trans. Geosci. Remote Sens.* **2017**, *55*, 777–786. [CrossRef]
52. Casu, F.; Elefante, E.; Imperatore, P.; Zinno, I.; Manunta, M.; De Luca, C.; Lanari, R. SBAS-DInSAR Parallel Processing for Deformation Time Series Computation. *IEEE JSTARS* **2014**, *7*, 3285–3296. [CrossRef]
53. Manunta, M.; De Luca, C.; Zinno, I.; Casu, F.; Manzo, M.; Bonano, M.; Fusco, A.; Pepe, A.; Onorato, G.; Berardino, P.; et al. The Parallel SBAS Approach for Sentinel-1 Interferometric Wide Swath Deformation Time-Series Generation: Algorithm Description and Products Quality Assessment. *IEEE Trans. Geosci. Remote Sens.* **2019**, *57*, 6259–6281. [CrossRef]
54. De Luca, C.; Cuccu, R.; Elefante, S.; Zinno, I.; Manunta, M.; Casola, V.; Rivolta, G.; Lanari, R.; Casu, F. An On-Demand Web Tool for the Unsupervised Retrieval of Earth's Surface Deformation from SAR Data: The P-SBAS Service within the ESA G-POD Environment. *Remote Sens.* **2015**, *7*, 15630–15650. [CrossRef]
55. Morishita, Y.; Lazecky, M.; Wright, T.J.; Weiss, J.R.; Elliott, J.R.; Hooper, A. LiCSBAS: An Open-Source InSAR Time Series Analysis Package Integrated with the LiCSAR Automated Sentinel-1 InSAR Processor. *Remote Sens.* **2020**, *12*, 424. [CrossRef]
56. González, P.J.; Walters, R.J.; Hatton, E.L.; Spaans, K.; McDougall, A.; Hooper, A.J.; Wright, T.J. LiCSAR: Tools for automated generation of Sentinel-1 frame interferograms. In Proceedings of the AGU Fall Meeting 2016, San Francisco, CA, USA, 12–16 December 2016.

57. Yu, C.; Li, Z.; Penna, N.T.; Crippa, P. Generic atmospheric correction model for Interferometric Synthetic Aperture Radar observations. *J. Geophys. Res. Solid Earth* **2018**, *123*, 9202–9222. [CrossRef]
58. Foumelis, M.; Blasco, J.M.D.; Brito, F.; Pacini, F.; Pishehvar, P. Snapping for Sentinel-1 Mission on Geohazards Exploitation Platform: An Online Medium Resolution Surface Motion Mapping Service. In Proceedings of the 2021 IEEE International Geoscience and Remote Sensing Symposium IGARSS, Brussels, Belgium, 11–16 July 2021; pp. 3991–3994. [CrossRef]
59. Crosetto, M.; Solari, L.; Mróz, M.; Balasis-Levinsen, J.; Casagli, N.; Frei, M.; Oyen, A.; Moldestad, D.A.; Bateson, L.; Guerrieri, L.; et al. The Evolution of Wide-Area DInSAR: From Regional and National Services to the European Ground Motion Service. *Remote Sens.* **2020**, *12*, 2043. [CrossRef]
60. Costantini, M.; Minati, F.; Trillo, F.; Ferretti, A.; Novali, F.; Passera, E.; Dehls, J.; Larsen, Y.; Marinkovic, P.; Eineder, M.; et al. European Ground Motion Service (EGMS). In Proceedings of the International Symposium on Geoscience and Remote Sensing (IGARSS), Brussels, Belgium, 11–16 July 2021; pp. 3293–3296. [CrossRef]
61. Papoutsis, I.; Kontoes, C.; Alatza, S.; Apostolakis, A.; Loupasakis, C. InSAR Greece with Parallelized Persistent Scatterer Interferometry: A National Ground Motion Service for Big Copernicus Sentinel-1 Data. *Remote Sens.* **2020**, *12*, 3207. [CrossRef]
62. Hooper, A.; Segall, P.; Zebker, H. Persistent scatterer interferometric synthetic aperture radar for crustal deformation analysis, with application to Volcán Alcedo, Galápagos. *J. Geophys. Res.* **2007**, *112*, B07407. [CrossRef]
63. Bekaert, D.P.S.; Walters, R.J.; Wright, T.J.; Hooper, A.J.; Parker, D.J. Statistical comparison of InSAR tropospheric correction techniques. *Remote Sens. Environ.* **2015**, *170*, 40–47. [CrossRef]
64. Wang, Y.; Guo, Y.; Hu, S.; Li, Y.; Wang, J.; Liu, X.; Wang, L. Ground Deformation Analysis Using InSAR and Backpropagation Prediction with Influencing Factors in Erhai Region, China. *Sustainability* **2019**, *11*, 2853. [CrossRef]
65. Cohen-Waeber, J.; Bürgmann, R.; Chaussard, E.; Giannico, C.; Ferretti, A. Spatiotemporal patterns of precipitation-modulated landslide deformation from independent component analysis of InSAR time series. *Geophys. Res. Lett.* **2018**, *45*, 1878–1887. [CrossRef]
66. Ponziani, F.; Ciuffi, P.; Bayer, B.; Berni, N.; Franceschini, S.; Simoni, A. Regional-scale InSAR investigation and landslide early warning thresholds in Umbria, Italy. *Eng. Geol.* **2023**, *327*, 107352. [CrossRef]
67. Liu, Y.; Qiu, H.; Yang, D.; Liu, Z.; Ma, S.; Pei, Y.; Zhang, J.; Tang, B. Deformation responses of landslides to seasonal rainfall based on InSAR and wavelet analysis. *Landslides* **2022**, *19*, 199–210. [CrossRef]

Disclaimer/Publisher's Note: The statements, opinions and data contained in all publications are solely those of the individual author(s) and contributor(s) and not of MDPI and/or the editor(s). MDPI and/or the editor(s) disclaim responsibility for any injury to people or property resulting from any ideas, methods, instructions or products referred to in the content.